Decomposing the Dynamics of Delayed Hodgkin-Huxley Neurons

Gábor Orosz

Abstract. The effects of time delays on the nonlinear dynamics of neural networks are investigated. A decomposition method is utilized to derive modal equations that allow one to analyze the dynamics around synchronous states. The D-subdivision method is used to study the stability of equilibria while the stability of periodic orbits is investigated using Floquet theory. These methods are applied to a system of delay coupled Hodgkin-Huxley neurons to map out stable and unstable synchronous states. It is shown that for sufficiently strong coupling there exist delay ranges where stable equilibria coexist with stable oscillations which allow neural systems to respond to different environmental stimuli with different spatiotemporal patterns.

1 Introduction

Since Hodgkin and Huxley has constructed the first biophysical model of a neuron more than six decades ago [6] the field of neuroscience has gone through a enormous development. This led to detailed understanding of the dynamical phenomena underlying signal generation and propagation on neural membranes [4]. When modeling these processes, nonlinear ordinary differential equations (ODEs) are used to describe the voltage changes and ion transport at a given location of the membrane, while to describe the activity on the surface of the entire neuron partial differential equations (PDEs) are required. Additional ODEs can be used to describe the chemical processes at the synapses where signals are transmitted between neurons. Indeed, such detailed models are not feasible when modeling the behavior of populations of neurons. In this case, simplifications are often made so that neurons are considered to be "point-wise" and the couplings are considered to be instantaneous, that is, the infinite-dimensional dynamics of signal propagation is neglected. In this paper, we

Gábor Orosz
Department of Mechanical Engineering, University of Michigan,
Ann Arbor, MI 48109 USA
e-mail: orosz@umich.edu

T. Vyhlídal, J.-F. Lafay, and R. Sipahi (eds.), *Delay Systems*,
Advances in Delays and Dynamics 1,
DOI: 10.1007/978-3-319-01695-5_25,

consider an extended modeling framework for neural networks where neurons are still point-wise but signal propagation is modeled by inserting time delays into the coupling functions. This leads to delay differential equations (DDEs) which retain the essential infinite dimensional dynamics of signal transmission while the models remain scalable for large numbers of neurons and connections.

In order to understand the behavior of the resulting large interconnected delayed systems, we decompose the dynamics and derive modal equations in the vicinity of synchronous states. In particular, we focus on synchronous equilibria and periodic oscillations. The decomposition method used here can also be extended to more general cluster states [11] while other methods may be used when studying traveling wave solutions [2, 8]. Similar decomposition methods have been used to investigate the synchronized states in neural networks and laser networks [3, 5] and to study the dynamics of communication protocols [1, 9]. We remark that in the former case stability is usually determined numerically by calculating Lyapunov exponents while the latter case focuses on linear systems. In this paper, we apply rigorous mathematical techniques from dynamical systems theory to analyze the nonlinear dynamics of large interconnected systems.

As the result of the modal decomposition we obtain linear delay differential equations of small size. One of these modal equations describes the stability of synchronous states within the infinite-dimensional synchronization manifold which is called *tangential stability*. The other modal equations correspond to braking the synchrony, that is, they describe the so-called *transversal stability*; see [11, 12]. When considering the modal equations around equilibria, they have time-independent coefficients and consequently the D-subdivision method and Stépán's formulae [15] can be used to derive analytical stability charts. Each modal equation produces a set of stability curves and crossing these curves lead to different oscillatory solutions. For periodic oscillations the modal equations have time-periodic coefficients, that is, one needs to use Floquet theory [7] to evaluate stability. Tangential stability can be evaluated by restricting the dynamics to the synchronization manifold. For transversal stability, augmented systems are created so that each system consists of the nonlinear synchronous equation and a linear transversal modal equation.

In this paper, we apply these techniques to systems of delay coupled Hodgkin-Huxley neurons considering different connectivity structures. We derive the bifurcation structure arising within the synchronization manifold and show that this structure is independent of the connectivity and the number of oscillators in the system when the coupling strength is scaled appropriately. On the other hand, transversal bifurcations of equilibria and periodic orbits are influenced by the coupling structure. We demonstrate that for appropriate values of time delay and coupling strength, stable synchronous equilibrium coexist with stable oscillations. In this case, applying different external perturbations the system approaches different spatiotemporal patterns that can be exploited when encoding information.

2 Decomposition of Delayed Networks around Synchronous States

In this paper, we consider a system consisting of N identical oscillators coupled by identical couplings:

$$\dot{x}_i(t) = f\big(x_i(t)\big) + \frac{1}{N}\sum_{j=1}^{N} a_{ij}\, g\big(x_i(t), x_j(t-\tau)\big)\,, \tag{1}$$

for $i = 1,\ldots,N$, where the internal state of node i is described by the vector $x_i \in \mathbb{R}^n$ and the internal dynamics consist of a set of nonlinear ODEs $\dot{x}_i = f(x_i)$. The couplings are described by the function $g(x_i, x_j)$ that depends on the states of the interacting nodes. The time delay τ is the time needed for the signal transmission processes to take places. The coupling structure of the system is captured by a directed graph, whose elements are represented by the coefficients of the N-dimensional adjacency matrix

$$a_{ij} = \begin{cases} 1 & \text{if node } j \text{ is connected to node } i, \\ 0 & \text{otherwise,} \end{cases} \tag{2}$$

for $i, j = 1,\ldots,N$. Referring to the graph representation of the network, the oscillators are often called nodes and the connections between them called edges. Here, we use the abbreviated notation $A_N = [a_{ij}]$ and assume that A_N is diagonalizable, that is, if an eigenvalue has algebraic multiplicity m then it also has geometric multiplicity m, resulting in m linearly independent eigenvectors. The methods presented below may still be used when this condition does not hold but the algebraic calculations become more involved. We remark that equation (1) requires an infinite dimensional state space and the initial conditions are functions on the time interval $[-\tau, 0]$.

In this paper, we focus on the synchronous state

$$x_i(t) = x_{\mathrm{s}}(t)\,, \quad i = 1,\ldots,N\,. \tag{3}$$

Substituting (3) into (1) results in the delay differential equation

$$\dot{x}_{\mathrm{s}}(t) = f\big(x_{\mathrm{s}}(t)\big) + \frac{M}{N}\, g\big(x_{\mathrm{s}}(t), x_{\mathrm{s}}(t-\tau)\big)\,, \tag{4}$$

where the row sum

$$M = \sum_{j=1}^{N} a_{ij}\,, \tag{5}$$

must be the same for every i to ensure the existence of synchronous solutions. We remark that equation (3) still requires an infinite dimensional state space, that is, the *synchronization manifold* defined by (3) is infinite dimensional. Equation (4) may produce a variety of different behaviors, e.g., equilibria, periodic orbits, and even

chaotic motion. Here we focus on the first two cases. Synchronized equilibria are defined by

$$x_{\mathrm{s}}(t) \equiv x_{\mathrm{s}}^{*}\,, \tag{6}$$

and substituting this into (4) results in

$$0 = f\left(x_{\mathrm{s}}^{*}\right) + \frac{M}{N}\, g\left(x_{\mathrm{s}}^{*}, x_{\mathrm{s}}^{*}\right), \tag{7}$$

that is, the delay does not influence the location of equilibria (but may influence their stability). On the other hand, synchronous periodic oscillations satisfy

$$x_{\mathrm{s}}^{\mathrm{p}}(t) = x_{\mathrm{s}}^{\mathrm{p}}(t + T_{\mathrm{p}})\,, \tag{8}$$

where T_{p} represents the period. These can be determined by solving the boundary value problem comprised of (4) and (8) and the shape and stability of these orbits are influenced by the delay.

We define the perturbations $y_i = x_i - x_{\mathrm{s}}$ for $i = 1,\ldots,N$, so the linearization of (1) about the synchronous solution (3) can be written as

$$\dot{y}_i(t) = L y_i(t) + R \sum_{j=1}^{N} a_{ij}\, y_j(t-\tau)\,, \tag{9}$$

for $i = 1,\ldots,N$. When linearizing about the synchronous equilibrium (6), the $n \times n$ matrices L, R are time-independent, that is,

$$L^{*} = Df\left(x_{\mathrm{s}}^{*}\right) + \frac{M}{N} D^{(1)} g\left(x_{\mathrm{s}}^{*}, x_{\mathrm{s}}^{*}\right), \qquad R^{*} = \frac{1}{N} D^{(2)} g\left(x_{\mathrm{s}}^{*}, x_{\mathrm{s}}^{*}\right), \tag{10}$$

where and $D^{(1)}$ and $D^{(2)}$ represent derivatives with respect to the first and second variables, respectively. In this case, (9) gives a linear time-invariant system allowing the use of analytical techniques like the D-subdivision method and Stépán's formulae [15] to determine the stability of the equilibrium. However, when linearizing about synchronous oscillations (8), the matrixes L, R in (9) become time-periodic with period T_{p}, that is,

$$\begin{aligned} L(t) &= Df\left(x_{\mathrm{s}}^{\mathrm{p}}(t)\right) + \frac{M}{N} D^{(1)} g\left(x_{\mathrm{s}}^{\mathrm{p}}(t), x_{\mathrm{s}}^{\mathrm{p}}(t-\tau)\right) = L(t + T_{\mathrm{p}})\,, \\ R(t) &= \frac{1}{N} D^{(2)} g\left(x_{\mathrm{s}}^{\mathrm{p}}(t), x_{\mathrm{s}}^{\mathrm{p}}(t-\tau)\right) = R(t + T_{\mathrm{p}})\,. \end{aligned} \tag{11}$$

Thus, one must use Floquet theory to evaluate the stability of oscillations. The corresponding monodromy operators usually cannot be written in closed form and consequently, numerical techniques like full discretization [14] or semi-discretization [7] are needed.

Using $\mathbf{y} = \mathrm{col}\,[y_1 \;\; y_2 \;\; \ldots \;\; y_N] \in \mathbb{R}^{nN}$ the linear system (9) can be rewritten as

$$\dot{\mathbf{y}}(t) = (I_N \otimes L)\,\mathbf{y}(t) + (A_N \otimes R)\,\mathbf{y}(t-\tau)\,, \tag{12}$$

where I_N is the N-dimensional unit matrix and A_N is the adjacency matrix. In order to decompose system (12) we construct the coordinate transformation

$$\mathbf{y} = (T_N \otimes I)\mathbf{z}, \tag{13}$$

where $\mathbf{z} = \mathrm{col}[z_1 \quad z_2 \quad \dots \quad z_N] \in \mathbb{R}^{nN}$, I is the $n \times n$ unit matrix, while $T_N = [e_1 \quad e_2 \quad \dots \quad e_N]$ where e_i is the i-th eigenvector of the adjacency matrix A_N. This transformation yields the linear modal equations

$$\dot{z}_i(t) = Lz_i(t) + \Lambda_i R z_i(t-\tau), \tag{14}$$

for $i = 1,\dots,N$, where Λ_i is the i-th eigenvalue of the adjacency matrix A_N. Note the due to the constant row sum (5), we have $\Lambda_1 = M$ and $e_1 = \mathrm{col}[1 \quad \dots \quad 1]$. The corresponding modal equation is indeed the linearization of (4) and it describes the *tangential stability*: stability against perturbations that keep the synchronous configuration. The other modal equations for $i = 2,\dots N$ describe *transversal stability*: stability against perturbations that split the synchronous configuration; see [11, 12]. We remark that for $\Lambda_{i,i+1} = \Sigma_i \pm \mathrm{i}\Omega_i \in \mathbb{C}$, defining $\xi_i = \mathrm{Re}\, z_i$, $\eta_i = -\mathrm{Im}\, z_i$ and taking the real and imaginary parts of (14) leads to the $2n$-dimensional real system

$$\begin{bmatrix} \dot{\xi}_i(t) \\ \dot{\eta}_i(t) \end{bmatrix} = \begin{bmatrix} L & O \\ O & L \end{bmatrix} \begin{bmatrix} \xi_i(t) \\ \eta_i(t) \end{bmatrix} + \begin{bmatrix} \Sigma_i R & \Omega_i R \\ -\Omega_i R & \Sigma_i R \end{bmatrix} \begin{bmatrix} \xi_i(t-\tau) \\ \eta_i(t-\tau) \end{bmatrix}, \tag{15}$$

where O represents the n-dimensional matrix with zero elements.

In this paper, we consider $N = 5$. For all-to-all coupling (without self coupling) the adjacency matrix, its eigenvalues, and the transformation matrix (given by the eigenvectors) can be written as

$$A_5 = \begin{bmatrix} 0&1&1&1&1 \\ 1&0&1&1&1 \\ 1&1&0&1&1 \\ 1&1&1&0&1 \\ 1&1&1&1&0 \end{bmatrix} \quad \Rightarrow \quad \begin{cases} \Lambda_1 = 4, \\ \Lambda_2 = -1, \\ \Lambda_3 = -1, \\ \Lambda_4 = -1, \\ \Lambda_5 = -1, \end{cases} \qquad T_N = \begin{bmatrix} 1&1&1&1&1 \\ 1&-1&0&0&0 \\ 1&0&-1&0&0 \\ 1&0&0&-1&0 \\ 1&0&0&0&-1 \end{bmatrix}. \tag{16}$$

Here the row sum is $M = N - 1 = 4$ (cf. (5)) and the transversal eigenvalue has multiplicity M. We will also consider the adjacency matrix

$$A_5 = \begin{bmatrix} 0&1&0&1&1 \\ 0&0&1&1&1 \\ 1&1&0&0&1 \\ 1&0&1&0&1 \\ 1&1&0&1&0 \end{bmatrix} \quad \Rightarrow \quad \begin{cases} \Lambda_1 = 3, \\ \Lambda_2 = 0, \\ \Lambda_3 = -1, \\ \Lambda_4 = -1+\mathrm{i}, \\ \Lambda_5 = -1-\mathrm{i}, \end{cases} \qquad T_N = \begin{bmatrix} 1&1&1&1&1 \\ 1&-2&1&\frac{-2+6\mathrm{i}}{5}&\frac{-2-6\mathrm{i}}{5} \\ 1&-2&1&\frac{-1-7\mathrm{i}}{5}&\frac{-1+7\mathrm{i}}{5} \\ 1&1&1&\frac{-8-\mathrm{i}}{5}&\frac{-8+\mathrm{i}}{5} \\ 1&1&-3&1&1 \end{bmatrix}, \tag{17}$$

where $M = 3$ and all eigenvalues are distinct.

2.1 Stability of Synchronous Equilibria and Periodic Orbits

As mentioned above, when linearizing about synchronous equilibria (6), the matrices L, R are time independent, cf. (10). Thus, in order to determine stability, the trial solutions $z_i(t) = Z_i \mathrm{e}^{\lambda t}$, $\lambda \in \mathbb{C}$, $Z_i \in \mathbb{C}^n$ are substituted into (14), which result in the characteristic equations

$$\det\left(\lambda I - L - \Lambda_i R \mathrm{e}^{-\lambda\tau}\right) = 0\,, \tag{18}$$

for $i = 1,\ldots,N$. When all the infinitely many characteristic roots λ are located in the left-half complex plane for $i = 1$ and $i = 2,\ldots N$, the equilibrium is tangentially and transversally stable, respectively. Substituting $\lambda = \mathrm{i}\omega$, $\omega \geq 0$ into the above equation one may obtain the tangential and transversal stability boundaries that divide the parameter space into stable and unstable domains. For each domain, stability can be evaluated by applying Stépán's formulae [15]. When crossing a tangential stability boundary the synchronized configuration is kept by the arising oscillations while crossing a transversal boundary gives rise to asynchronous oscillatory solutions.

When linearizing about the synchronized oscillations (8), the matrices L, R are time-periodic with period T_p, cf. (11). Instead of exponential trial solutions one must use Floquet theory to determine stability [7]. This requires the reformulation (14) using the state variables $z_{i,t}(\theta) = z_i(t+\theta)$, $\theta \in [-\tau, 0]$ that are contained by the infinite-dimensional space of continuous functions. These states can be obtained from the initial functions as

$$z_{i,t} = \mathscr{U}_i(t)\, z_{i,0}\,, \tag{19}$$

using the solutions operators $\mathscr{U}_i(t)$ for $i = 1,\ldots,N$. The eigenvalues of the monodromy operators $\mathscr{U}_i(T_\mathrm{p})$, called Floquet multipliers, determine the tangential and transversal stability of oscillations. If all these multipliers are smaller than 1 in magnitude, then the periodic solution is stable. As the monodromy operators cannot be written into closed form, one needs to use numerical techniques to determine the stability boundaries. First, we compute the periodic orbit which is the solution of the boundary value problem (4,8) using numerical collocation. Then using arc-length continuation we find the orbit when parameters are varied; see [14] for details. For $i = 1$, (14) is the linearization of (4) and collocations provide a discretization of the monodromy operator $\mathscr{U}_1(T_\mathrm{p})$ in (19) which allows the computation of the tangential Floquet multipliers. However, for $i = 2,\ldots N$, to obtain the transversal Floquet multipliers (i.e., the eigenvalues of $\mathscr{U}_i(T_\mathrm{p})$ for $i = 2,\ldots N$), the matrices in (14) or (15) have to be evaluated at the periodic solution. Thus, we create augmented systems consisting of (4,8) and a chosen equation of (14) or (15). The corresponding $2n$ or $3n$ dimensional equations possess a periodic orbit: the first n variables are equal to x_s^p while $z_i \equiv 0$ or $\xi_i = \eta_i \equiv 0$.

3 Synchrony of Delay Coupled Hodgkin-Huxley Neurons

Since the original work of Hodgkin and Huxley [6] a large number different models have been proposed to describe voltage activity and ion transport at the neural membrane (e.g., FitzHugh-Nagumo model, Morris-Lecar model); see [4]. As a matter of fact, these all originate form the Hodgkin-Huxley model which is still considered to be an etalon in neuro-dynamics. Here we consider Hodgkin-Huxley neurons coupled via direct electronic coupling called gap junctions; see [13]. (For the same model with synaptic coupling see [8].)

The time evolution of the system is given by the delay differential equations

$$\begin{aligned} C\dot{V}_i(t) &= I - g_{\mathrm{Na}} m_i^3(t) h_i(t) \big(V_i(t) - V_{\mathrm{Na}}\big) - g_{\mathrm{K}} n_i^4(t) \big(V_i(t) - V_{\mathrm{K}}\big) \\ &\quad - g_{\mathrm{L}} \big(V_i(t) - V_{\mathrm{L}}\big) + \frac{\kappa}{N} \sum_{j=1}^{N} a_{ij} \big(V_j(t-\tau) - V_i(t)\big)\,, \\ \dot{m}_i(t) &= \alpha_m\big(V_i(t)\big)\big(1 - m_i(t)\big) - \beta_m\big(V_i(t)\big) m_i(t)\,, \\ \dot{h}_i(t) &= \alpha_h\big(V_i(t)\big)\big(1 - h_i(t)\big) - \beta_h\big(V_i(t)\big) h_i(t)\,, \\ \dot{n}_i(t) &= \alpha_n\big(V_i(t)\big)\big(1 - n_i(t)\big) - \beta_n\big(V_i(t)\big) n_i(t)\,, \end{aligned} \tag{20}$$

for $i = 1, \ldots, N$, where the time t is measured in ms, the voltage of the i-th neuron at the soma V_i is measured in mV, and the dimensionless gating variables $m_i, h_i, n_i \in [0,1]$ characterize the "openness" of the sodium and potassium ion channels embedded in the cell membrane. The conductances g_{Na}, g_{K}, g_{L} and the reference voltages V_{Na}, V_{K}, V_{L} for the sodium channels, potassium channels and the so-called leakage current are given together with the membrane capacitance C and the driving current I in the appendix of [13]. The equations for m_i, h_i, n_i are based on measurements and the nonlinear functions $\alpha_m(V)$, $\alpha_h(V)$, $\alpha_n(V)$, $\beta_m(V)$, $\beta_h(V)$, $\beta_n(V)$ are also given in the appendix of [13]. The coupling term $\frac{\kappa}{N}\big(V_j(t-\tau) - V_i(t)\big)$ represents a direct electronic connection between the axon of the j-th neuron and the dendrites of the i-th neuron. Here $V_i(t)$ is the postsynaptic potential, $V_j(t-\tau)$ is the presynaptic potential, κ is the conductance of the gap junction, and τ represents the signal propagation time along the axon of the j-th neuron (dendritic delays are omitted here). That is, the presynaptic potential is equal to what the potential of the soma of the j-th neuron was τ time before.

For $\kappa = 0$ the neurons are uncoupled. In this case, there exist a unique stable oscillatory state where neurons spike periodically (with period $T_{\mathrm{p}} \approx 11.57$ ms), see the green curves in Fig. 1. The equation that describes the dynamics on the infinite dimensional synchronization manifold can be obtained by substituting

$$[V_i \;\; m_i \;\; h_i \;\; n_i] = [V_{\mathrm{s}} \;\; m_{\mathrm{s}} \;\; h_{\mathrm{s}} \;\; n_{\mathrm{s}}]\,, \qquad i = 1, \ldots, N\,, \tag{21}$$

into (20); cf. (3,4). In this case, the coupling term becomes $\kappa\frac{M}{N}\big(V_{\mathrm{s}}(t-\tau) - V_{\mathrm{s}}(t)\big)$. Notice that this term disappears for $\tau = 0$, that is, the synchronized motion is the same as the uncoupled one. However, this does not hold for $\tau > 0$.

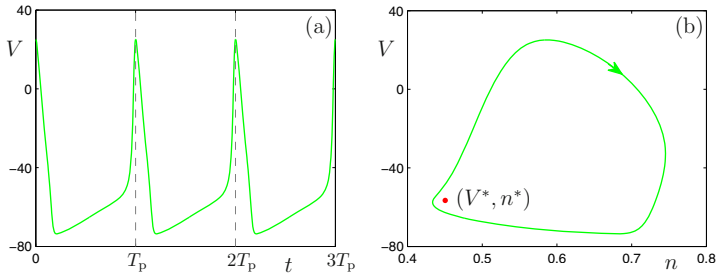

Fig. 1 Stable periodic solution of model (20) without coupling $\kappa = 0$. Panel (a) shows the periodic variation of the membrane voltage V as a function of time t (with period $T_p \approx 11.57$ ms) while panel (b) depicts the periodic orbit in state space. The red dot represents the unstable equilibrium.

When linearizing (20) about (21) one obtains the matrixes

$$L = \begin{bmatrix} -p - \frac{M}{N}\frac{\kappa}{C} & -a_1 & -a_2 & -a_3 \\ -b_1 & -c_1 & 0 & 0 \\ -b_2 & 0 & -c_2 & 0 \\ -b_3 & 0 & 0 & -c_3 \end{bmatrix}, \quad R = \begin{bmatrix} \frac{1}{N}\frac{\kappa}{C} & 0 & 0 & 0 \\ 0 & 0 & 0 & 0 \\ 0 & 0 & 0 & 0 \\ 0 & 0 & 0 & 0 \end{bmatrix}, \tag{22}$$

where

$$\begin{aligned} p &= (g_{\mathrm{Na}} m_{\mathrm{s}}^3 h_{\mathrm{s}} + g_{\mathrm{K}} n_{\mathrm{s}}^4 + g_{\mathrm{L}})/C\,, \\ a_1 &= g_{\mathrm{Na}} 3 m_{\mathrm{s}}^2 h_{\mathrm{s}} (V_{\mathrm{s}} - V_{\mathrm{Na}})/C\,, & b_1 &= -\alpha_m'(V_{\mathrm{s}})(1 - m_{\mathrm{s}}) + \beta_m'(V_{\mathrm{s}}) m_{\mathrm{s}}\,, \\ a_2 &= g_{\mathrm{Na}} m_{\mathrm{s}}^3 (V_{\mathrm{s}} - V_{\mathrm{Na}})/C\,, & b_2 &= -\alpha_h'(V_{\mathrm{s}})(1 - h_{\mathrm{s}}) + \beta_h'(V_{\mathrm{s}}) h_{\mathrm{s}}\,, \\ a_2 &= g_{\mathrm{K}} 4 n_{\mathrm{s}}^3 (V_{\mathrm{s}} - V_{\mathrm{K}})/C\,, & b_3 &= -\alpha_n'(V_{\mathrm{s}})(1 - n_{\mathrm{s}}) + \beta_n'(V_{\mathrm{s}}) n_{\mathrm{s}}\,, \\ c_1 &= \alpha_m(V_{\mathrm{s}}) + \beta_m(V_{\mathrm{s}})\,, & c_2 &= \alpha_h(V_{\mathrm{s}}) + \beta_h(V_{\mathrm{s}})\,, & c_3 &= \alpha_n(V_{\mathrm{s}}) + \beta_n(V_{\mathrm{s}})\,, \end{aligned} \tag{23}$$

that appear in the linear equation (9,12) as well as in the modal equations (14,15).

3.1 *Stability of Synchronous Equilibria*

Let us consider synchronized equilibria, that is, $[V_{\mathrm{s}}(t) \quad m_{\mathrm{s}}(t) \quad h_{\mathrm{s}}(t) \quad n_{\mathrm{s}}(t)] \equiv [V_{\mathrm{s}}^* \quad m_{\mathrm{s}}^* \quad h_{\mathrm{s}}^* \quad n_{\mathrm{s}}^*]$. At this state the coupling term disappears and consequently the synchronized equilibrium is the same as the equilibrium of an uncoupled neuron. For parameters defined in [13] we have a unique equilibrium as shown by the red dot in Fig. 1(b). Moreover, the matrices (22) become constant (cf. (10)) and the characteristic equation (18) leads to

$$\lambda^4 + d_1\lambda^3 + d_2\lambda^2 + d_3\lambda + d_4 + \tfrac{1}{N}\tfrac{\kappa}{C}\left(M - \Lambda_i \mathrm{e}^{\lambda\tau}\right)\left(\lambda^3 + \tilde{c}_1\lambda^2 + \tilde{c}_2\lambda + \tilde{c}_3\right) = 0\,, \tag{24}$$

where

$$\begin{aligned}
&\tilde{c}_1 = c_1 + c_2 + c_3\,, \qquad \tilde{c}_2 = c_1c_2 + c_1c_3 + c_2c_3\,, \qquad \tilde{c}_3 = c_1c_2c_3\,,\\
&d_1 = p + \tilde{c}_1\,,\\
&d_2 = p\tilde{c}_1 + \tilde{c}_2 - \big(a_1b_1 + a_2b_2 + a_3b_3\big)\,,\\
&d_3 = p\tilde{c}_2 + \tilde{c}_3 - \big(a_1b_1(c_2+c_3) + a_2b_2(c_1+c_3) + a_3b_3(c_1+c_2)\big)\,,\\
&d_4 = p\tilde{c}_3 - \big(a_1b_1c_2c_3 + a_2b_2c_1c_3 + a_3b_3c_1c_2\big)\,,
\end{aligned} \tag{25}$$

that are evaluated at $V_{\rm s}(t) \equiv V_{\rm s}^*$. Substituting $\lambda = {\rm i}\omega$ into (24), separating the real and imaginary parts, and using some algebraic manipulations one may obtain the stability boundaries in the (τ,κ)-plane parameterized by the angular frequency ω. In particular, considering $\Lambda_1 = M$ results in the tangential boundaries

$$\begin{aligned}
&\tau = \frac{2}{\omega}\left\{\arctan\left[-\frac{\alpha(\omega)}{\beta(\omega)}\right] + \ell\pi\right\}, \qquad \ell = 0,1,2,\ldots\\
&\kappa = -\frac{CN}{2M}\frac{\alpha^2(\omega)+\beta^2(\omega)}{\alpha(\omega)\gamma(\omega)}\,,
\end{aligned} \tag{26}$$

where

$$\begin{aligned}
&\alpha(\omega) = (d_1 - \tilde{c_1})\omega^6 + (d_2\tilde{c}_1 + \tilde{c}_3 - d_3 - d_1\tilde{c}_2)\omega^4 + (d_3\tilde{c}_2 - d_2\tilde{c}_3 - d_4\tilde{c}_1) + d_4\tilde{c}_3\,,\\
&\beta(\omega) = -\omega^7 + (d_2 + \tilde{c}_2 - d_1\tilde{c}_1)\omega^5 + (d_1\tilde{c}_3 + d_3\tilde{c}_1 - d_4 - d_2\tilde{c}_2) + (d_4\tilde{c}_2 - d_3\tilde{c}_3)\omega\,,\\
&\gamma(\omega) = \omega^6 + (\tilde{c}_1^2 - 2\tilde{c}_2)\omega^4 + (\tilde{c}_2^2 - 2\tilde{c}_1\tilde{c}_3)\omega^2 + \tilde{c}_3^2\,.
\end{aligned} \tag{27}$$

Similarly for $\Lambda_i \in \mathbb{R}$ one may obtain the transversal boundaries

$$\begin{aligned}
&\tau = \frac{2}{\omega}\left\{\arctan\left[\frac{1}{M+\Lambda_i}\frac{\alpha(\omega)}{\beta(\omega)}\Big(-\Lambda_i \pm \sqrt{\Delta}\Big)\right] + \ell\pi\right\}, \qquad \ell = 0,1,2,\ldots\\
&\kappa = \frac{CN}{M^2-\Lambda_i^2}\frac{\alpha(\omega)}{\gamma(\omega)}\Big(-M \mp \sqrt{\Delta}\Big)\,,
\end{aligned} \tag{28}$$

where

$$\Delta = \Lambda_i^2 - \big(M^2 - \Lambda_i^2\big)\frac{\beta^2(\omega)}{\alpha^2(\omega)}\,. \tag{29}$$

For $\Lambda_i = \Sigma_i + {\rm i}\Omega_i \in \mathbb{C}$ the first equation in (28) changes to

$$\tau = \frac{2}{\omega}\left\{\arctan\left[\frac{1}{M+\Sigma_i+\Omega_i\frac{\alpha(\omega)}{\beta(\omega)}}\frac{\alpha(\omega)}{\beta(\omega)}\left(-\Sigma_i + \Omega_i\frac{\beta(\omega)}{\alpha(\omega)} \pm \sqrt{\Delta}\right)\right] + \ell\pi\right\}, \tag{30}$$

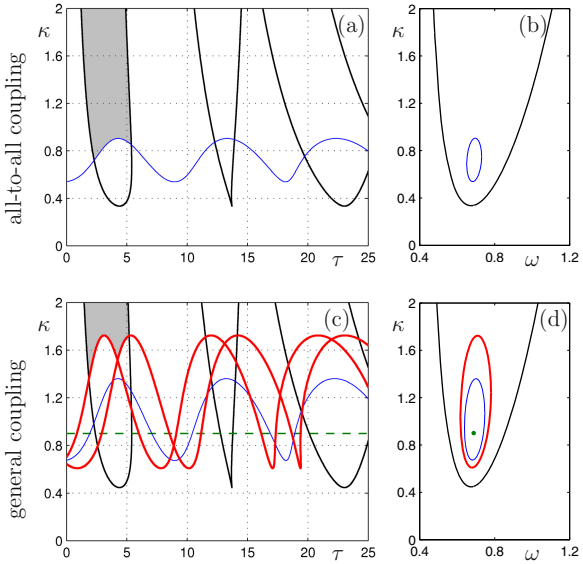

Fig. 2 Stability charts corresponding to the formulae (26,28,30,31) are shown in panels (a,c) and the corresponding angular frequencies are shown in panels (b,d). The top and bottom rows correspond the adjacency matrices (16) and (17), respectively. The stable domain is shaded, black "lobe shaped" curves represent tangential boundaries for $\Lambda_1 = M$, and colored "wavy" curves represent transversal boundaries for $\Lambda_2 = -1$ — thin blue, $\Lambda_3 = 0$ — dashed green, and $\Lambda_{4,5} = -1 \pm \mathrm{i}$ — thick red.

and $\Lambda_i^2 = \Sigma_i^2 + \Omega_i^2$. Finally, we remark that for $\Lambda_i = 0$ the boundary is given by

$$\kappa = -\frac{CN}{M}\frac{\alpha(\omega^*)}{\gamma(\omega^*)}, \tag{31}$$

where ω^* is the solution of $\beta(\omega^*) = 0$, that is, this boundary is delay independent.

The corresponding curves are plotted for $N = 5$ in the (τ, κ)-plane in Fig. 2(a) and (c) for the coupling matrixes (16) and (17), respectively. The tangential stability boundaries are shown as black curves and these form lobes. One may observe that in (26) τ is independent of the number of oscillators N and the row sum M while κ is proportional to N/M. Corresponding to this the lobes in Fig. 2(c) are the "stretched" versions of the lobes in Fig. 2(a). The transversal boundaries are shown as colored curves and for each transversal eigenvalue Λ_i the boundary appears as a "wavy" curve. For all-to-all coupling there is only one transversal curve corresponding to the multiplicity of the modal eigenvalues in (16). For general coupling (17) there are four distinct curves: the horizontal dashed green line corresponds to the zero modal eigenvalue, the thin blue curve corresponds to the real modal eigenvalue while the thick red curves correspond to the complex conjugate pair of modal eigenvalues. Notice that the larger the magnitude of the transverse modal eigenvalue is, the larger the "amplitude" of the "wavy" curve is.

The stability of the synchronized equilibrium changes via Andronov-Hopf bifurcation when crossing either a tangential or a transversal stability curve. That is a pair of complex conjugate eigenvalues crosses the imaginary axis leading to oscillations. The corresponding frequencies are shown in Fig. 2(b) and (d). One may observe that along the tangential lobes the frequency changes with κ in the interval $\omega \in [0,\infty)$. On the other hand, frequencies along tangential boundaries are contained in a closed interval that increases with the magnitude of the transversal eigenvalue. Applying the analytical stability criteria [15], it can be shown that the system is tangentially stable within in the leftmost lobe while transversal stability of each mode can be guaranteed when choosing parameters above the corresponding "wavy" curve. Thus the equilibrium is linearly stable in the shaded domain that appears to be larger for the all-to-all coupled network.

3.2 Stability of Synchronous Periodic Orbits

As shown above, the modal equations (14,15) with matrices (22) allow one to determine the stability of equilibria in a systematic way. However, neural systems encode information using rhythmic patterns which correspond to periodic oscillations. To derive synchronous oscillations, one must solve (20,21) when considering $[V_\mathrm{s}(t)\ \ m_\mathrm{s}(t)\ \ h_\mathrm{s}(t)\ \ n_\mathrm{s}(t)] = [V_\mathrm{s}(t+T_\mathrm{p})\ \ m_\mathrm{s}(t+T_\mathrm{p})\ \ h_\mathrm{s}(t+T_\mathrm{p})\ \ n_\mathrm{s}(t+T_\mathrm{p})]$, where T_p is the period of oscillations. We use the numerical continuation package DDE-BIFTOOL [14] to follow branches of periodic solutions when varying parameters. To evaluate the stability of these solutions we use the nonlinear equation describing the dynamics on the synchronization manifold (i.e., (20) with restriction (21)) and augment this with a modal equation from (14) or (15).

The left and right columns of Fig. 3 show the bifurcation diagrams for the adjacency matrices (16) and (17), respectively. Each panel depicts the peak-to-peak voltage amplitude $|V_\mathrm{s}|$ as a function of the time delay τ while the value of the coupling strength κ is indicated on each panel. The horizontal axis represents the synchronized equilibrium. Solid green and dashed red curves represent stable and unstable states, respectively. Bifurcations are marked as stars (Hopf and Neimark-Sacker), crosses (fold and pitchfork), and diamonds (period doubling). The color of the marker indicates which mode becomes unstable: black symbols indicate tangential stability losses while green, blue and red symbols corresponds to zero, real and complex conjugate modal eigenvalues, cf. Fig. 2. For simplicity we only mark the bifurcations where the stability of a mode changes.

Notice that the structure of the bifurcation diagrams and the tangential stability losses are the same for all-to-all and general coupling when rescaling the κ values by $4/3$; cf. (4). For weak coupling the equilibrium is tangentially unstable while the periodic orbit is tangentially stable for all values of τ; see panels (a) and (f). For stronger coupling the equilibrium may loose its tangential stability via Hopf bifurcations (black stars) corresponding to the lobes in Fig. 2 and the arising oscillations stay within the synchronization manifold; see panels (c–e) and (h–j). Oscillatory solutions may undergo tangential fold bifurcations (black crosses) leading to

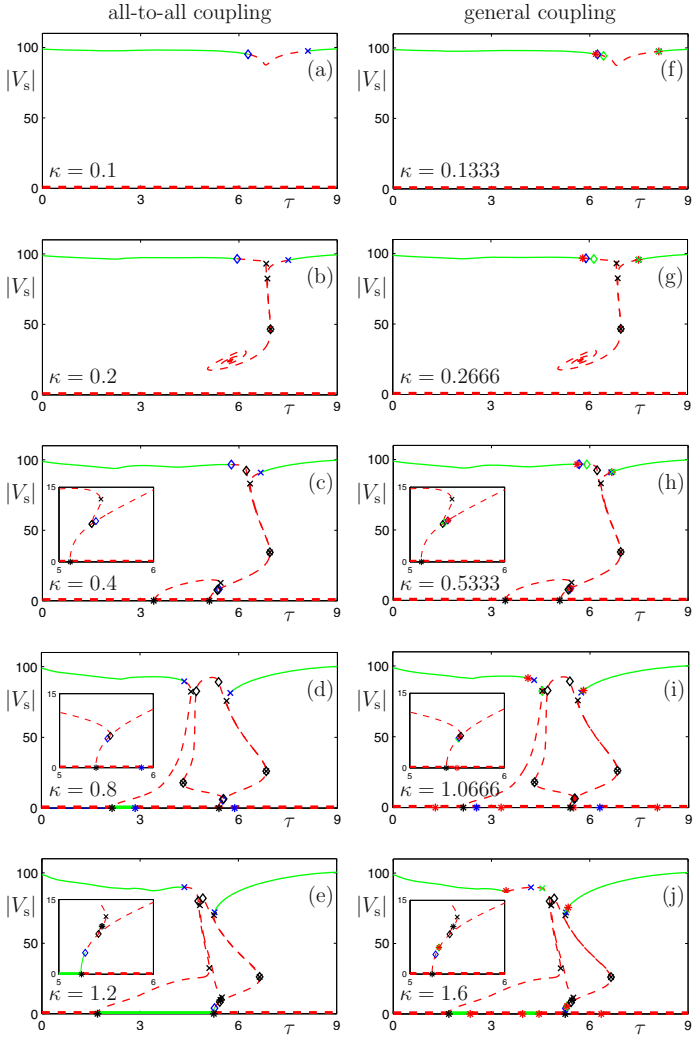

Fig. 3 Bifurcation diagrams showing the peak-to-peak voltage amplitude $|V_s|$ of synchronized oscillations as a function of the delay τ for different values of the coupling strength κ. The left and right columns correspond to the adjacency matrices (16) and (17), respectively. The horizontal axis represents the equilibrium. Stable and unstable states are depicted by solid green and dashed red curves. Stars represent Hopf bifurcations of equilibria or Neimark-Sacker bifurcations of periodic orbits, crosses represent fold or pitchfork bifurcations, and diamonds denote period doubling bifurcations. The color of symbols distinguishes between the modes; see the caption of Fig. 2.

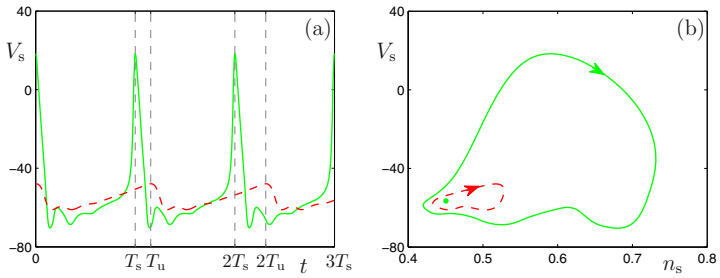

Fig. 4 Stable (solid green) and unstable (dashed red) periodic orbits corresponding to $\tau = 3$ ms and $\kappa = 1.2$ mS/cm^2; cf. Fig. 3(e). The corresponding periods are $T_s \approx 15.39$ ms and $T_u \approx 17.78$ ms.

coexisting T_p-periodic solutions. For a range of κ a cascade of fold bifurcations is observed that culminate in single point where $T_p \to \infty$; see the spiral in panels (b) and (g). Tangential period doubling (flip) bifurcations (black diamonds) give rise to branches of $2T_p$-periodic oscillations that are typically tangentially unstable. (These are not depicted in the figures). Also, co-dimension two fold-flip bifurcations can be observed when the coupling is sufficiently strong; see panels (b–e) and (g–h). For strong coupling tangential Neimark-Sacker bifurcations (black stars) result in quasi-periodic oscillations; see panels (e) and (j). (Such oscillations cannot be traced with the current state-of-the-art techniques).

The equilibrium may also loose its transversal stability via Hopf bifurcations (colored stars) corresponding to the "wavy" curves in Fig. 2. The oscillations arising trough these bifurcations brake the synchrony. For synchronous oscillations, transversal stability losses may occur via pitchfork bifurcations (colored crosses), via period doubling bifurcations (colored diamonds), and via Neimark-Sacker bifurcations (colored stars). Corresponding to the multiplicity of modal eigenvalues each transversal boundary found for (16) splits into three for (17), so that stability is typically lost to the mode with complex conjugate modal eigenvalues (that are the largest in magnitude) via Neimark-Sacker bifurcation (red stars).

For strong coupling one may observe domains where stable synchronized equilibrium coexist with stable and unstable synchronized oscillations. These domains arise via subcritical Hopf bifurcations and, depending on the initial conditions, the system may approach the equilibrium or the periodic solution. Such orbits are depicted in Fig. 4. When comparing this figure with Fig. 1 one may notice the changes in the shape of the stable (solid green) periodic orbit. Moreover, the period of stable oscillations ($T_s \approx 15.39$ ms) and the period of unstable oscillations ($T_u \approx 17.78$ ms) exceed the period of the uncoupled oscillations ($T_p \approx 11.57$ ms). We remark that there exist additional stable periodic solutions corresponding to different cluster states that can be approached by the system for certain initial conditions but these are not investigated in this paper; see [11] for more details.

4 Conclusion and Discussion

Systems of delay coupled Hodgkin-Huxley neurons were studied in this paper and the dynamics of synchronized states were mapped out when varying the coupling strength and the coupling delay. The dynamics were decomposed and modal equations of small size were derived that describe the tangential and transversal dynamics in the vicinity of the synchronous equilibria and oscillations. These equations allowed us to characterize the synchronous dynamics and determine the regions where the system approaches synchronized states. The most important outcome of the analysis is that when the coupling is strong enough there exist delay ranges where stable synchronized equilibria coexist with stable oscillations. We remark that for simplified neural models such multi-stability may not occur [10] which emphasizes the importance of models that are based on biophysical measurements.

While in this paper we only mapped out synchronous oscillations, detailed investigations show that many different cluster oscillations may also exist in these domains [11]. That is, depending on the initial conditions, the neural system may approach the synchronous equilibrium (which is a homogenous rest state) or different oscillatory states corresponding to different spatiotemporal patterns. As external stimuli can "reset the initial condition", the multi-stable dynamics discovered allow the neural system to respond to different external stimuli with different spatiotemporal patterns which is crucial for encoding environmental information. Note that such domains only exist for sufficiently large time delays which emphasizes that delays cannot be neglected when modeling neural networks. In fact, our results suggest that nature may tune the delays in large interconnected biological systems so that the information encoding capabilities of organisms are maximized.

References

1. Cepeda-Gomez, R., Olgac, N.: An exact method for the stability analysis of linear consensus protocols with time delay. IEEE Transactions on Automatic Control 56(7), 1734–1740 (2011)
2. Coombes, S.: Neuronal networks with gap junctions: a study of piecewise linear planar neuron models. SIAM Journal on Applied Dynamical Systems 7(3), 1101–1129 (2008)
3. D'Huys, O., Fischer, I., Danckaert, J., Vicente, R.: Role of delay for the symmetry in the dynamics of networks. Physical Review E 83(4), 046223 (2011)
4. Ermentrout, G.B., Terman, D.H.: Mathematical Foundations of Neuroscience. In: Interdisciplinary Applied Mathematics., vol. 35, Springer (2010)
5. Flunkert, V., Yanchuk, S., Dahms, T., Schöll, E.: Synchronizing distant nodes: a universal classification of networks. Physical Review Letters 105(25), 254101 (2010)
6. Hodgkin, A.L., Huxley, A.F.: A quantitative description of membrane current and its application to conduction and excitation in nerve. Journal of Physiology 117(4), 500–544 (1952)
7. Insperger, T., Stépán, G.: Semi-discretization for Time-delay Systems: Stability and Engineering Applications. Applied Mathematical Sciences, vol. 178. Springer (2011)
8. Kantner, M., Yanchuk, S.: Bifurcation analysis of delay-induced patterns in a ring of Hodgkin-Huxley neurons. Philosophical Transactions of the Royal Society A (to appear, 2013)

9. Olfati-Saber, R., Murray, R.M.: Consensus problems in networks of agents with switching topology and time-delays. IEEE Transactions on Automatic Control 49(9), 1520–1533 (2004)
10. Orosz, G.: Decomposing the dynamics of delayed networks: equilibria and rhythmic patterns in neural systems. In: Sipahi, R. (ed.) 10th IFAC Workshop on Time Delay Systems, pp. 173–178. IFAC (2012)
11. Orosz, G.: Decomposition of nonlinear delayed networks around cluster states with applications to neuro-dynamics. SIAM Journal on Applied Dynamcal Systems (submitted, 2013)
12. Orosz, G., Moehlis, J., Ashwin, P.: Designing the dynamics of globally coupled oscillators. Progress of Theoretical Physics 122(3), 611–630 (2009)
13. Orosz, G., Moehlis, J., Murray, R.M.: Controlling biological networks by time-delayed signals. Philosophical Transactions of the Royal Society A 368(1911), 439–454 (2010)
14. Roose, D., Szalai, R.: Continuation and bifurcation analysis of delay differential equations. In: Krauskopf, B., Osinga, H.M., Galan-Vioque, J. (eds.) Numerical Continuation Methods for Dynamical Systems, Understanding Complex Systems, pp. 359–399. Springer (2007)
15. Stépán, G.: Retarded Dynamical Systems: Stability and Characteristic Functions. Pitman Research Notes in Mathematics, vol. 210. Longman (1989)